EJNMMI Reports

ORIGINAL ARTICLE Open Access

Quantitative assessment of kidney split function and mean transit time in healthy patients using dynamic ^{18}F-FDG PET/MRI studies with denoising and deconvolution methods making use of Legendre polynomials

Michel Destine[1*] and Alain Seret[2]

*Correspondence: michel.destine@chuuclnamur.uclouvain.be

[1] Nuclear Medicine Department, Sainte Elisabeth Hospital, CHU UCL Namur, Namur, Belgium
[2] GIGA Research - CRC Human Imaging Unit, University of Liège, Liège, Belgium

Abstract

Purpose: Our objective was to assess a deconvolution and denoising technique based on Legendre polynomials compared to matrix deconvolution on dynamic ^{18}F-FDG renography of healthy patients.

Method: The study was carried out and compared to the data of 24 healthy patients from a published study who underwent examinations with ^{99m}Tc-MAG3 planar scintigraphy and ^{18}F-FDG PET/MRI. Due to corruption issues in some data used in the published article, post-publication measurements were provided. We have been warned that post-publication data were treated differently. The smoothing method switched from Bezier to Savitzky–Golay and the deconvolution from matrix-based (with Tikhonov Regularization) to Richardson–Lucy. A comparison of the split function and mean transit times of the published and post-publication data against our method based on Legendre polynomials was performed.

Results: For split function, we only observed a good agreement between the processing methods for the ^{99m}Tc-MAG$_3$ and the post-published data. No correlation was found between the split functions obtained on the ^{99m}Tc-MAG$_3$ and the ^{18}F-FDG, contrary to the published study. However, all calculated split function values for ^{18}F-FDG and ^{99m}Tc-MAG$_3$ were within the established normal range. For the mean transit time, the correlation was moderate with published data and very good with the post-publication measurements for both ^{99m}Tc-MAG$_3$ and ^{18}F-FDG. Bias of the Bland–Altman analysis of the mean transit times for ^{99m}Tc-MAG$_3$ versus ^{18}F-FDG was 1.1 min (SD 1.7 min) for the published data, − 0.11 min (SD 1.9 min) for the post-publication results and .05 min (SD 1.9 min) for our method.

Conclusions: The processing methods used in the original publication and in the post-publication work were quite complex and required adaptation of the fitting parameters for each individual and each type of examination. Our method did not require any specific adjustment; the same unmodified and fully automated algorithm was successfully applied to all data.

Keywords: PET-MRI, MAG_3, FDG, Kidneys, Split function, Mean transit time, Deconvolution, Legendre polynomials

Background

Positron emission tomography (PET) is part of nuclear medicine procedures. Beyond the distinct type of radiotracer—positron emitter—used, it also differs from other nuclear medicine examinations—planar scintigraphy and single photon emission computed tomography (SPECT) imaging—by the technology and design used, which may offer some advantages. Among them, we can find a better spatiotemporal resolution, an absolute quantification of the radiolabeled tracer, the possibility of a dynamic 3D acquisition, a high sensitivity—down to pico-molar concentration—and the possibility to reduce drastically the amount of radiotracer needed for the examination. Nowadays, PET systems are conventionally coupled with CT or MRI scanners which provide anatomical data allowing more precise regions of interest to be drawn, to better localize lesions or to correct for partial volume effect. PET is used mainly by neurologists, cardiologists, and oncologists, but its use extends progressively to other areas. An example is the development of new renal radiotracers (Werner et al. 2019). The kidney is not anymore only considered for its influence on the washout, quantification, or distribution of the PET radiotracer into the body but also for the possibility of determining its filtration capabilities, monitoring its function during chemotherapy, radiolabeled therapy, or assessing living donor kidney before transplant and to the recipient.

The most widely used tracer in PET is [^{18}F] 2-deoxy-2-fluoro-D-glucose (FDG), and recently a team from the Medical University of Vienna came up with the following question: could FDG be used to evaluate kidney function?

FDG is filtered at the glomerulus and partially reabsorbed in the proximal tubule, whereas we have glomerular filtration and tubular secretion for the standard scintigraphy tracer, [^{99m}Tc] Mercaptoacetyltriglycine (MAG_3). The time-activity curves (Fig. 1) for the two tracers are quite dissimilar as a result of this physiological difference between ^{99m}Tc-MAG_3 and ^{18}F-FDG. Another possible issue of using PET is that the axial field of view of classical systems (15–25 cm) cannot encompass the entire urinary tract in one field of view as allowed by the large field of view of a standard gamma-camera. But this limitation could disappear in the forthcoming years if we consider the recent development of extended axial field of view PET systems (up to 1 m and above) (Alberts et al. 2023).

As in scintigraphy, noise is present in PET data, and a noise reduction method is generally mandatory before most data processing. Among them is the deconvolution, which is known to be very sensitive to noise (Kenny et al. 1975; Diffey et al. 1976; Destine et al. 2020).

In previous studies (Destine et al. 2020, 2022), we implemented an automatic denoising and deconvolution solution for ^{99m}Tc-MAG_3 time-activity curves. The method uses Legendre polynomials transformation and an analysis of the Legendre coefficient spectrum involved in the Legendre transformation. We are now aiming to assess the possible extension of the method to the evaluation of the kidney split function and mean transit time from data obtained with dynamic FDG PET.

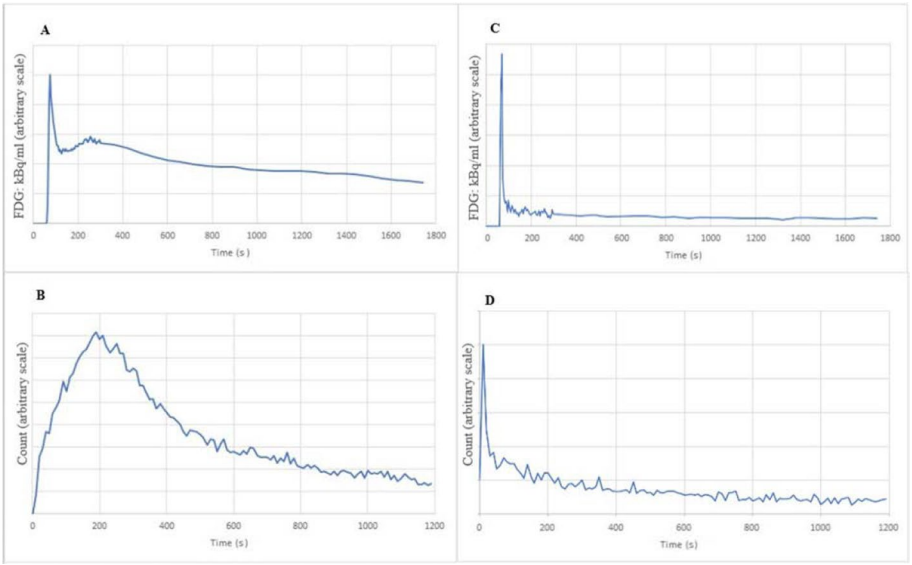

Fig. 1 FDG (**A**) and MAG_3 (**B**) time-activity curves for the same healthy kidney and the FDG (**C**) and MAG_3 (**D**) associated input function. The frame rate for the MAG_3 is 10 s, and for the FDG is composed of 60 images of 5 s followed by 25 images of 60 s

Materials and methods

Ethical Institutional Review Board approval was obtained, and the requirement to obtain informed consent was waived for this study because of its retrospective nature. The original studies were in accordance with the ethics committee of the University of Vienna (acceptance no. 1068/2015).

Anonymized data from the 24 studies used in the original publication (Geist et al. 2019) of Geist B.K. et al. (BKG) were received. Due to storage problems, only both MAG_3 and FDG raw data from 16 studies out of the 24 used by BKG could be retrieved. Nevertheless, the authors were able to provide the results of their post-publication measurements for the split function and mean transit times for the MAG_3 and FDG studies of all 24 subjects as well as the raw TAC extracted from the kidneys and aorta ROIs drawn on the PET FDG images (without partial volume effect correction).

The studies were dynamic kidney exploration with MAG_3 planar scintigraphy and FDG PET/MRI of 24 adult subjects (average age 39 ± 14 years). For both studies, the patients were hydrated and instructed to empty their bladder before the tracer injection. The MAG_3 acquisition parameters followed the recommendations of the European Association of Nuclear Medicine (EANM 2011) (Gordon et al. 2011). It was acquired with a frame rate of 10 s for 30 min and an injected activity of about 80 MBq. The PET/MRI (Siemens Biograph mMR, Siemens Germany) was performed 9 ± 5 days after or before the MAG_3 with an injection of FDG of 3 MBq/kg body weight. The PET duration was of 30 min. The recorded list mode file was re-binned into a sequence of 60×5 s followed by another of 25×60 s. The reconstruction was performed into a $172 \times 172 \times 127$ matrix for a total of 10,795 images. The MRI examination included a T1 VIBE SPAIR sequence used for volume delineation, attenuation, and partial volume effect corrections.

Determination of split function and mean transit time

The split function (SF) was determined by integrating the first 1–2 min of the time-activity curve for MAG_3 and FDG but also the 1–3 min for FDG. Indeed, Geist et al. (2019) deduced that a better correlation between the reference SF_{MAG3} and SF_{FDG} was obtained when the integration of the FDG TAC was taken for minutes 1 to 3 compared to the 1 to 2 min. We also obtained SF_{FDG} from the plateau height ratio of the curves obtained by deconvolution of the kidney TAC by the input function (Destine et al. 2022).

The values of reference for the relative left renal uptake were taken from the MAG_3 1–2 min integral method. For the 16 MAG_3 studies with retrieved images, blood, whole-kidneys, and background regions were drawn (Fig. 2A) and analysed with the Hermes renogram analysis software (version 2.6Q; Hermes Medical Solutions AB, Stockholm, Sweden). The Regions of interest were exported in xml format for further analysis with our in-house software (Destine et al. 2020). The kidney background ROIs were drawn from the lateral direction, going from the lower to the upper pole to avoid pelvi-ureteric activity. A ROI was drawn over the left ventricle to obtain the input function.

For the FDG images, the delineation of the kidneys and aorta was performed simultaneously on the PET and MRI images (Fig. 2B) with the LIFEx software (LIFEx version V7.3.0, Paris, France). The ROIs were drawn manually on each slice. The part of the aorta chosen was between the diaphragm and the arteria renalis, according to the original choice of Geist et al. (2018, 2019). Three aorta regions were created: the MRI structure of the aorta, the PET activity and an expended 2D region with the dilate tool in the LIFEx program. For all the ROIs—kidneys and aorta—the PET different time bins were explored for the best possible delineation. The TAC of each structure was exported in units of kBq/ml. No background subtraction was applied for the 3D PET. A comparison of the TACs received from BKG and those exported from LIFEx was carried out.

The first zero points of the TAC were trimmed since the PET acquisition started immediately after the injection of the radiotracer.

Due to the lack of original raw data for some subjects, two types of comparison were done. One—called partial—with the subset of data (16 subjects) were both the original MAG_3 and FDG images were available, and one—called provided values (pv)—for all 24 subjects where we used the TAC FDG datasets provided. The reason was to be able to extrapolate the results obtained with the reduced dataset and improve the statistical evaluation.

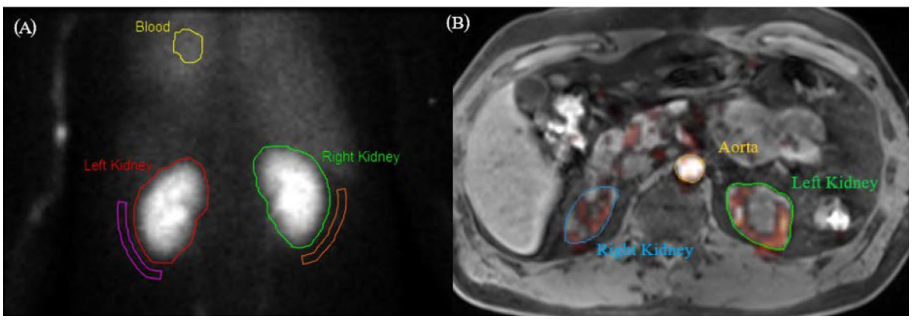

Fig. 2 **A** MAG_3 regions of interest (ROIs) over the heart for blood input function, whole left and right kidneys, and their respective backgrounds. **B** MRI T1 and PET images, fused at the FDG peak activity within the aorta. ROIs are manually delineated for the aorta, left kidney, and right kidney

As we observed some intriguing discrepancies between our results and the measurements provided by BKG, we used the two Bland–Altman—split function and mean transit time (MTT) of FDG vs MAG_3—graphs of the original article (Geist et al. 2019) to retrieve the individual SF and MTT (called reverse BA SF and BA MTT) obtained with both tracers for each patient. This was straightforward as it only required to resolve a system of two equations with two unknowns and a positive matrix determinant which guarantees the solution's existence and unicity.

Partial volume effects correction

On the fused PET/MRI images, FDG activity was visible outside the MRI contour of the aorta. The presence of the outside activity may be due to the combination of the partial volume effect (PVE) and the patient's internal motion. PVE is linked to the poor (compared to MRI) spatial resolution of PET. The transverse spatial resolution of the PET system used in the study is given by a FWHM @ 1 cm of 4.6 mm (manufacturer data). The average dimension of a normal descending aorta (Erbel 2006) is in first approximation 20–30 mm for men and even smaller for women, with an expansion rate of 1–2 mm per year. Many techniques are available to correct for PET PVE. But here, the correction applied will take advantage of the MRI delineation of the aorta, which gives a precise calculation of the volume. To perform the PVE correction, three regions of interest were used. One is given by the contour of the aorta observed on the MRI images which was used to determine the actual arterial volume. A second by a ROI drawn on PET images acquired a few seconds after injection in the range of the arterial input function (AIF) peak occurrence. A third one was obtained by expanding the previous FDG region by three PET voxels and used for background correction. The relationship between the 3 regions gives the final corrected concentration of FDG in the aorta (Khalighi et al. 2018). Both the corrected and uncorrected AIF were used in deconvolution (see below). This made it possible to obtain renal retention curves (RRC) and MTT with or without PVE.

Deconvolution

The PET TAC points were not evenly sampled, which is an issue for the deconvolution. An interpolation of the sparsely sampled points (second sequence of the PET acquisition) of the kidney and blood TAC was mandatory. This was done in two ways: through a simple linear interpolation—as BKG did—and via a slight adaptation of the Legendre transform going from approximation to interpolation (Fig. 3). The returned sparse Legendre polynomial obtained on the second sequence is simply used to calculate the interpolated points (Fig. 3). The Legendre interpolation method always offered a smoother curve.

The deconvolution of FDG and MAG_3 TACs was performed with our Legendre denoising and deconvolution technique (LG) according to the procedure described in our previous publications (Destine et al. 2020, 2022). The input function and the noisy renograms were denoised through the use of a finite Legendre representation (Destine et al. 2020) before LG. No other smoothing method was applied. The same method for MAG_3 and FDG for the starting point of the input curve was applied: the input curve peak time was taken as the zero time (Durand et al. 2008). The RRC plateau was calculated from the mean value (PMean) of the RRC curve between 1.2 and 2.0 min for

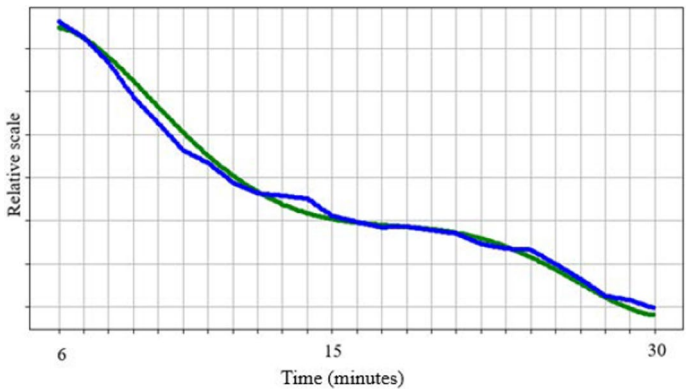

Fig. 3 Interpolation of the second sequence (6–30 min post injection) of 25 × 60 s into a sampling rate of 5 s using either a linear (blue line) or a Legendre (green line) interpolation method

MAG_3 and between 1.4 and 2.9 min for FDG. This slight shift of the time window for the plateau computation resulted from the presence of a broader vascular peak in the FDG RRC. This PMean replaced all the values from zero to the time point where the RRC fell below 85% of the PMean (Fleming 1988).

Finally, the FDG and MAG_3 TACs were visually inspected and compared to the calculated values by a physician trained for 12 years in nuclear medicine.

Statistical analysis

The mean, standard deviation (SD) and range were used to describe the spread of the measurements. Agreements between methods were assessed by the Bland–Altman method (Altman and Bland 1983). The slope, intercept, and coefficient of determination (R^2) were obtained from linear regression for pairwise comparison of the outcomes. Statistical tests were performed at a 5% level of significance ($p < 0.05$) using XLStat (version 2019.1.3).

Results

Extracted curves on raw data

Using the fused PET/MRI images, it was possible to extract for the partial raw data set TAC strictly identical to those provided by BKG. This validated the use of the complete set of provided TACs and therefore the MAG_3 and FDG data from the 24 subjects.

Partial volume correction

The partial volume effect was assessed on raw PET data. The diameter of the aorta measured on the MRI was on average 24.1 ± 3.32 mm. A good alignment between the aorta on MRI and FDG activity was seen (Fig. 2B). Supplemental Fig. S1 is a random pickup of TACs for ROI over the MRI and PET aorta showing an excellent visual correlation without any correction. Applying the PVE correction did not affect the results significantly. Since the aorta TAC curves provided by BKG are uncorrected, we kept in the following only the uncorrected values for strict comparison purposes.

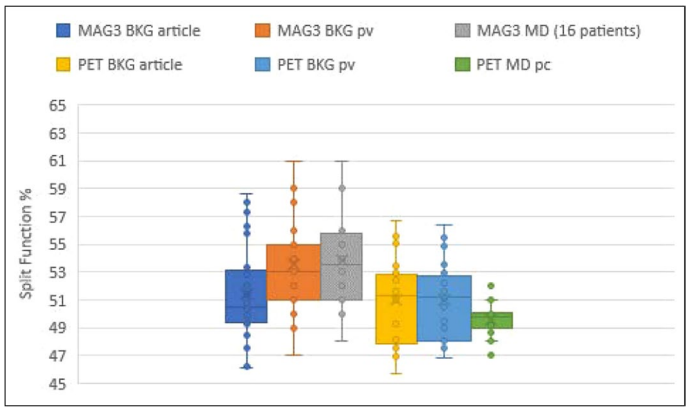

Fig. 4 Box-plot of MAG_3 split function (integral method) from BKG original article (blue), BKG provided values (orange) and our own measurement on partial raw data (grey), and the FDG split function from BKG article (yellow), BKG provided values (light blue) and our own measurement (integral method) on all the provided curves (green)

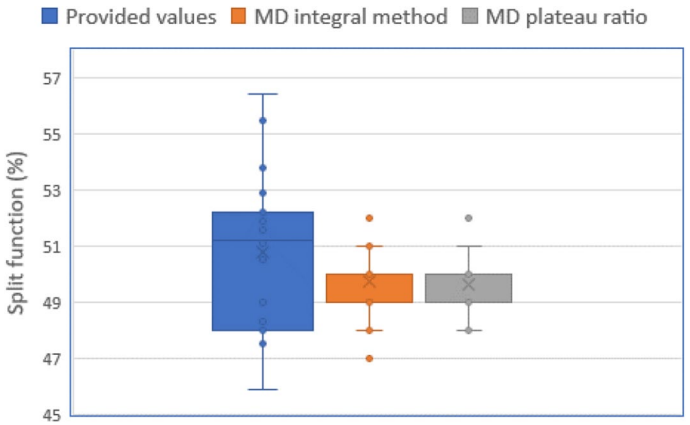

Fig. 5 Box-plot of PET split function for the 16 patients (integral method) from BKG (blue), MD integral method (orange) and MD plateau ratio (grey) of the RRC

Split function

Figure 4 summarizes the SF results obtained by BKG and our analysis. The Pearson correlation between the MAG_3 split function (SF_{MAG3}) from our measurement (MAG_3 MD) on the partial dataset and the measurement provided by BKG (MAG_3 BKG pv) for the same patients was good ($r = 0.93$). However, these provided SF_{MAG3} values showed a systematic positive difference from the published values (Geist et al. 2019). This systematic deviation was only observed for MAG_3. For the FDG split function (SF_{FDG}), the correlation between published and provided values was very good ($r = 0.99$, $p = 0.88$).

For FDG, there was no correlation between the BKG SF values (article or pv) and our (MD) computed values ($r = 0.27$) using either the integral method (Fig. 4) or the ratio of the plateau heights of the RRC after the Legendre deconvolution. For each patient, the SF_{FDG} obtained using our integral method or the plateau ratio always differed by less than 5%. Figure 5 illustrates the comparative analysis between the integral method and the plateau ratio method in calculating the FDG split function.

Mean transit time

When measured with Hermes software, the mean transit time for MAG_3 (MTT_{MAG3}) for the partial raw data (MD) and MTT_{MAG3} provided by BKG showed a good correlation (Fig. 6). The linear regression ends with a slope of 0.97, an intercept of 0.1 min and a $R^2 = 0.99$. There was also a good correlation between the values obtained with the Hermes software (MAG_3 MD 16 patients, MD MTT_{MAG3}) and MTT_{MAG3} obtained using our own Legendre based processing method (MAG_3 Legendre 16 patients, LG MTT_{MAG3}), confirming previous results (Destine et al. 2022). The correlation of LG MTT_{MAG3} with MD MTT_{MAG3} and with BKG MTT_{MAG3} pv was 0.98. However, discrepancies were found between the BKG provided and published MTT_{MAG3} values ($p = 0.01$) (Fig. 6).

The measure of the mean transit time for FDG (MTT_{FDG}) needed an interpolation of the data to ensure a constant sampling rate. The values of MTT_{FDG} computed with the linear or the Legendre interpolation method used for the second part of the acquisition (25×60 s) were not statistically significant ($p = 0.5$). The comparison of the MTT_{FDG} obtained by the Legendre method between the 16 measured patients TAC and the 24th provided curves was consistent and did not show outliers (Fig. 6).

The Bland–Altman analysis of the reverse BA MTT (Fig. 7) was very close to the BA analysis published by BKG (Geist et al. 2019) with bias of 1.1 min. However, it differed clearly from the BA analysis of the provided values (Fig. 8) where the bias was only − 0.11 min.

BA analysis of BKG MTT_{MAG3} provided values, and LG MTT_{FDG} values led to a bias close to zero for the entire dataset (Fig. 9). Applied to LG MTT_{MAG3} and LG MTT_{FDG} calculated on the partial dataset (Fig. 10), the BA analysis again conducted to a bias close to zero. Moreover, the distribution of the points in the two BA graphs (Figs. 9 and 10) was very similar. The BA analysis for the BKG and LG MTT_{FDG} for the 24 subjects showed a bias of − 0.04 min with SD less than 0.5 min (Fig. 11).

The results of these multiple Bland–Altman comparisons are summarized in Table 1.

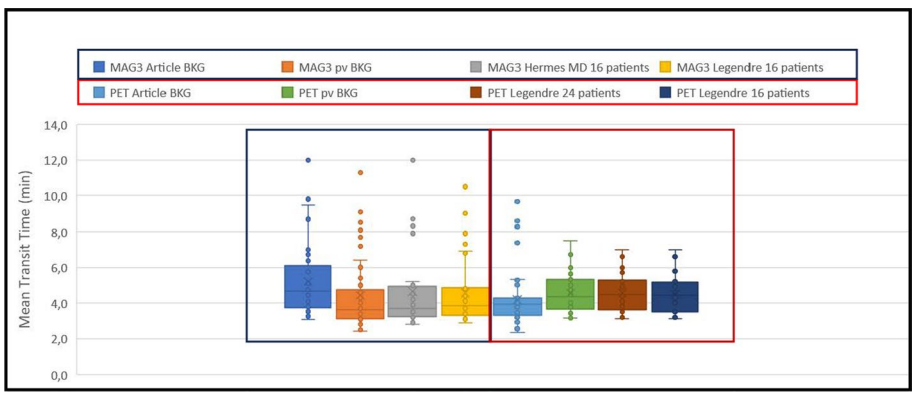

Fig. 6 Box-plot comparison of the values for MTT. From left to right, the first four boxes are for MAG_3 and respectively values found in BKG publication, provided by BKG after publication, computed in this study using Hermes and our own Legendre base software. The four last boxes are for FDG, and respectively values found in publication, provided by BKG and Legend method applied to all 24 subjects or to the partial subset of 16 patients

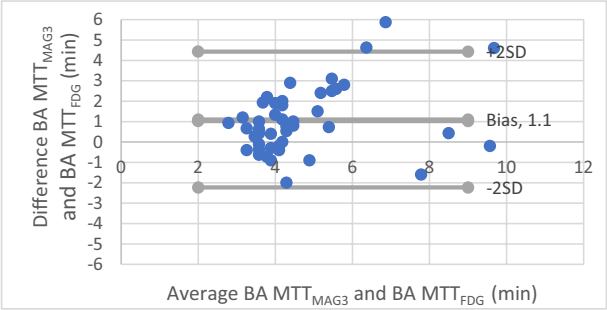

Fig. 7 Bland–Altman analysis of the MTT for MAG_3 and FDG from the original article reproduced after solving the BA equation. The grey lines represent two standard deviation (SD)

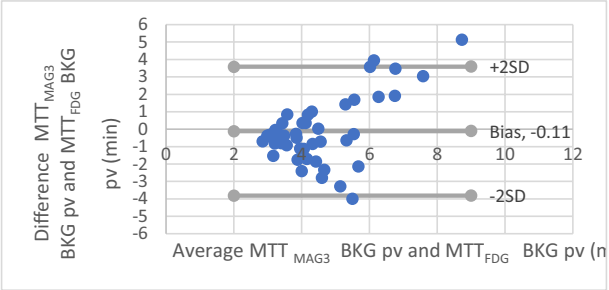

Fig. 8 Bland–Altman analysis of the MTT_{MAG3} and MTT_{FDG} for the BKG provided values

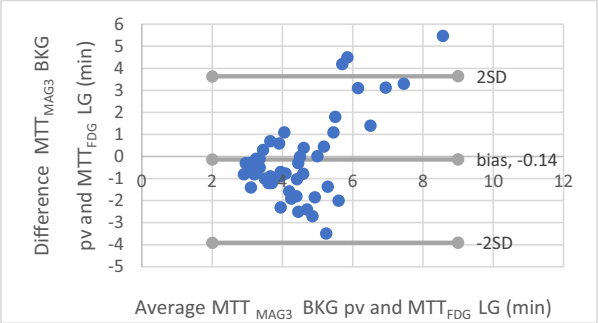

Fig. 9 Bland–Altman analysis of the MTT_{MAG3} values provided by BKG and the MTT_{FDG} computed with LG on all 24 provided curves

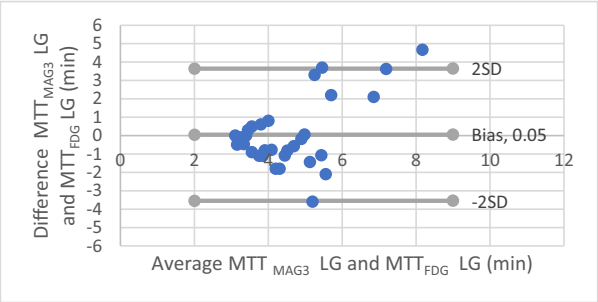

Fig. 10 Bland–Altman analysis applied to the raw data for the MTT_{MAG3} and MTT_{FDG} computed both by LG from raw images (16 patients)

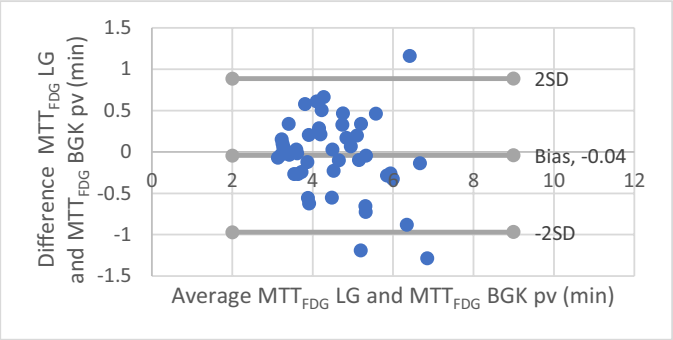

Fig. 11 Bland–Altman analysis of the MTT_{FDG} computed with LG on the provided curves and the MTT_{FDG} of the BKG provided values

Table 1 Summary of the Bland–Altman comparisons

Figures		Bias (min)	SD (min)
7	MTT_{MAG3} vs MTT_{FDG} BKG both from article	1.1	1.7
8	MTT_{MAG3} vs MTT_{FDG} BKG both from pv	−0.11	1.9
9	MTT_{MAG3} BKG pv vs MTT_{FDG} LG	−0.14	1.8
10	MTT_{MAG3} vs MTT_{FDG} LG (partial)	0.05	1.9
11	MTT_{FDG} LG vs MTT_{FDG} BKG	−0.04	0.5

Considering a MTT_{MAG3} value of 3.5 ± 1 min for the average normal hydrated patients (Durand et al. 2008), ten kidneys were found with a lengthened transit time. Six out of these kidneys had a lengthened MTT_{FDG} from the BKG pv results and seven from the LG method.

Discussion

The results published by BKG (Geist et al. 2019) were obtained with a rather cumbersome data processing. BKG has try to refine the whole processing in a subsequent but unpublished work. Following details kindly provided by BKG, the changes for MAG_3 concerned only new delineation of the ROIs, while for the FDG, the changes were deeper and as follows. The original contouring of the kidney was a little bit changed. The smoothing method applied to the TAC was shifted from the Bezier method to the Savitzki–Golay method. The deconvolution method also evolved. At the matrix deconvolution used for the publication, succeeded a matrix-based method with Tikhonov regularization and finally the Richardson–Lucy algorithm (Richardson 1972). It is here worth mentioning that the Tikhonov regularization required a manual adjustment of the regularization factor for each data set. With the latest version of her processing BKG obtained the TAC and results referenced in this work as the provided values.

On our side, we have recently developed for standard nuclear renography a fully automated processing including deconvolution based on Legendre polynomials that was successfully applied to normal and abnormal MAG_3 2D examinations (Destine et al. 2020, 2022). Our main objective in the present work was to explore if this method could be applied to 3D imaging as well and eventually with a tracer leading to TAC with a

different shape than the MAG_3. The study conducted by BKG with FDG fulfilled both conditions.

First of all, the lack of a significant difference between the TACs obtained with LIFEx from the raw PET images and those provided by BKG was an important starting point for comparing the processing methods despite the data storage issue in Vienna. This made possible to rely on the entire PET dataset with 24 patients and not only on the subgroup of 16 patients for which original PET data could be retrieved.

Whereas the locally obtained SF_{MAG3} with Hermes or our own Legendre based software correlated very well with the BKG provided SF_{MAG3}, they all appeared to be larger than those used by BKG in the original publication (Fig. 4). The mean SF_{MAG3} was 53.8% for the local results, 53.2% for BKG provided values and only 51.4% for the published values. We obtained very few variations in SF_{FDG} among the subjects, with a mean SF_{FDG} value of about 50%. More variability was found in BKG provided and published values (Figs. 4 and 5). To illustrate that we never could observe the SF_{MAG3} extreme values reported by BKG, we present as supplemental data (Fig. S2) the FDG TAC of the subject with the highest BKG SF_{MAG3} (61%). Visually and whatever the time gate (1–2 min. or 1–3 min.) used for the split function computation; a value largely different from 50% for SF_{FDG} is highly improbable. A similar observation was made for all other subjects. Due to all these differences, we could not retrieve the correlation between the split function obtained with MAG_3 and FDG described in the original article (Geist et al. 2019).

For the deconvolution process, the difference between linear and Legendre interpolation was not significant but may prove its interest in the presence of more noisy data. However, the concerned time domain was the tail of the TACs, with an increased time per frame, which is likely to have less influence on the final result.

For both tracers, the mean transit time values obtained with Legendre deconvolution are very similar to the BKG provided results (Figs. 6 and 11). LG can therefore be considered as efficient to compute MTT as the more complex algorithms successively used by BKG (Geist and Neufeld 2021). Moreover, LG has the following important additional advantage. Whereas the method was first developed and validated for MAG_3 in a context of 2D imaging, it could be applied to 3D PET data without any adaptation of the algorithm or any patient-by-patient fine tuning. If our and BKG pv MTT agree well for both tracers, they differ from the BKG published value (Fig. 6). Referring to the published values, MTT provided values were in mean lower by 1 min for MAG_3 and higher by about 0.5 min for FDG (Fig. 6). Both BKG pv results and our own results led to a very low bias in the MTT_{FDG} versus MTT_{MAG3} BA plots whereas the bias was much larger in the BKG original publication (Geist et al. 2019) (Table 1).

Referring to the provided values which were obtained using BKG optimized processing, our LG based methods delivered values in very good agreement for SF_{MAG3}, MTT_{MAG3} and MTT_{FDG} but SF_{FDG} values in mean slightly lower and much less dispersed. As pointed above, SF_{FDG} values very different from 50% are highly improbable when looking at the kidney TAC plots of these normal subjects. Also, the reported correlation (Geist et al. 2019) for the split function between MAG_3 and FDG was not observed with our results. It is our opinion that the SF range for both tracers obtained for these normal subjects is actually too narrow and that inclusion of subjects with impaired kidneys would be necessary. Such an extension of the study was out of scope

of our work. Additionally, several factors should also be considered before reaching any conclusion. Firstly, the kidney filtration of both tracers is quite different. FDG uptake occurs in both the renal cortex and medulla, as well documented in the literature (Rebelos et al. 2023; Dondi et al. 2023). Moreover, FDG uptake in extrarenal organs can affect image quality and potentially compromise in a processing dependent way the reliability of results. Additional corrections may therefore be necessary. Secondly, the MAG_3 images are 2D projections whereas PET provides 3D images for FDG that are corrected for attenuation and scatter. 2D scintigraphy images are not corrected for these physical effects and overlapping with other tissues does exist. This requires the use of background regions which is not the case for 3D images. In addition, the PET associated 3D MRI images help in the organ delineation.

Our study validated the correlation between mean transit time obtained with MAG_3 and FDG claimed by BKG but did not for the correlation of the split function. It therefore seems that additional studies would be needed before considering FDG as a straightforward clinical alternative to nuclear renography. Some other points should also be taken into account. The number of PET images is huge and may have low count statistics. A purely visual analysis of the numerous 2D PET cross-sections is not as simple as compared to planar MAG_3 images. Pseudo 2D planar images obtained from reprojection of the 3D PET images could maybe be considered as a mean for visual interpretation of these PET studies. Additionally, the shape of the curves obtained from the PET images are unusual for renograms and can be challenging to interpret for the physicians. For example, one of the trained physicians that coauthored our previous publication (Destine et al. 2022) was not able to find a visual correlation between the FDG TACs and the values obtained from the MAG_3. This held true even when the lengthened MTT was present in both FDG and MAG_3 studies or in the presence of large discrepancies between the SF.

Conclusions

Procedural guidelines for MAG_3 renography suggest to not rely on a single parameter but to visually evaluate the images and the extracted curves from them. Visually interpreting a large number of noisy PET images can be challenging. Additional parameters obtained by mathematical procedures are there to help the physician, and this is where the importance of having reliable quantifications comes in.

Here we successfully tested for the first case on 3D dynamic PET images a method based on finite Legendre polynomials representation, which was developed for 2D renography and is in our experience, quite simpler than those used later by BKG to process or reprocess the same data. The Legendre based method has the advantage of being fully automated and does not require adapting the fitting parameters. The results we are presenting were issued from our first processing of the curves.

The method was applied to PET ^{18}F-FDG, but could be fully applied to other more specific PET tracers—e.g. [18F]2-fluoro-2-deoxy-sorbitol (^{18}F-FDS)—which shows a more conventional assessment of human renal kinetics (Werner et al. 2019). Using the recently developed full ring CZT cameras, it could also be used for 3D dynamic renal scintigraphy analysis. Both would nevertheless require further investigation.

In summary, the LG method should be considered as a simple and reliable alternative method for routine analysis of renography in scintigraphy and PET.

Abbreviations

BA	Bland–Altman
FDG	Fluoro-deoxy-glucose
LG	Legendre deconvolution technique
PET	Positron emission tomography
MAG_3	Mercaptoacetyltriglycine
MRI	Magnetic resonance imaging
MTT	Mean transit time
Pmean	Plateau mean value of the renal retention curve
PV	Provided value
PVE	Partial volume effect
RRC	Renal retention curve
SF	Split function
TAC	Time-activity curve

Supplementary Information

The online version contains supplementary material available at https://doi.org/10.1186/s41824-024-00221-9.

Additional file 1.

Acknowledgements
We extend our heartfelt gratitude to Mag. Dr. rer. nat. B.K. Geist for providing images and post-publication results.

Author contributions
MD performed data collection analysis, mathematical development and produced the manuscript. AS contributed to the analysis of the results and contributed to the manuscript. All authors read and approved the final manuscript.

Funding
Not applicable.

Availability of data and materials
All data analyzed during this study are not publicly available due to data transfer agreement with the University of Vienna. The data may be obtained on reasonable request from Medical University of Vienna, Spitalgasse 23, 1090 Vienna Austria. Executing Department: Department of Biomedical Imaging and Image-guided Therapy, Währinger Gürtel 18-20, 1090 Vienna.

Declarations

Ethics approval and consent to participate
The ethical board at CHU UCL NAMUR (Reference ethics committee: 18/24) approved this retrospective study and waived the requirement for written consent.

Competing interests
Not applicable.

Received: 15 May 2024 Accepted: 2 September 2024
Published online: 15 October 2024

References

Alberts I, Sari H, Clemens M, Afshar-Oromieh A, Pyka T, Shi K et al (2023) Long-axial field-of-view PET/CT: perspectives and review of a revolutionary development in nuclear medicine based on clinical experience in over 7000 patients. Cancer Imaging 23(1):28. https://doi.org/10.1186/s40644-023-00540-3

Altman DG, Bland JM (1983) Measurement in medicine: the analysis of method comparison studies. Statistician 32(3):307. https://doi.org/10.2307/2987937

Destine M, Seret A (2020) Legendre polynomials: a fully automatic method for noise reduction in 99mTc-mercaptoacetyltriglycine renogram analysis. J Nucl Med Technol 48(4):346–353. https://doi.org/10.2967/jnmt.120.244574

Destine M, Hanin F-X, Mathieu I, Willemart B, Seret A (2022) Deconvolution of Tc-99m-mercaptoacetyltriglycine renograms with the concomitant use of a sparse Legendre polynomial representation and the Moore-Penrose pseudo-inverse. Mol Imaging Radionucl Ther. 31(1):7–15. https://doi.org/10.4274/mirt.galenos.2021.17363

Diffey BL, Hall FM, Corfield JR (1976) The 99mTc-DTPA dynamic renal scan with deconvolution analysis. J Nucl Med 17(5):352–355

Dondi F, Pisani AR, Lucarelli NM, Gazzilli M, Talin A, Albano D, Rubini D, Maggialetti N, Rubini G, Bertagna F (2023) Correlation between kidney uptake at [18F]FDG PET/CT and renal function. J Personal Med 14(1):40–40. https://doi.org/10.3390/jpm14010040

Durand E, Blaufox MD, Britton KE, Carlsen O, Cosgriff P, Fine E et al (2008) International scientific committee of radionuclides in nephrourology (ISCORN) consensus on renal transit time measurements. Semin Nucl Med 38(1):82–102. https://doi.org/10.1053/j.semnuclmed.2007.09.009

Erbel R (2006) Aortic dimensions and the risk of dissection. Heart 92(1):137–142. https://doi.org/10.1136/hrt.2004.055111

Fleming JS (1988) Functional radionuclide imaging of renal mean transit time and glomerular filtration rate. Nucl Med Commun 9:85–96. https://doi.org/10.1097/00006231-198802000-00004

Geist BK, Neufeld H (2021) Particle-number conservation, causality and linear response in biomedical imaging. Appl Math Comput 409(126418):126418. https://doi.org/10.1016/j.amc.2021.126418

Geist BK, Baltzer P, Fueger B, Hamboeck M, Nakuz T, Papp L et al (2018) Assessing the kidney function parameters glomerular filtration rate and effective renal plasma flow with dynamic FDG-PET/MRI in healthy subjects. EJNMMI Res 8(1):1–9. https://doi.org/10.1186/s13550-018-0389-1

Geist BK, Baltzer P, Fueger B, Hamboeck M, Nakuz T, Papp L et al (2019) Assessment of the kidney function parameters split function, mean transit time, and outflow efficiency using dynamic FDG-PET/MRI in healthy subjects. Eur J Hybrid Imaging 3(1):1–12. https://doi.org/10.1186/s41824-019-0051-9

Gordon I, Piepsz A, Sixt R (2011) Guidelines for standard and diuretic renogram in children. Eur J Nucl Med Mol Imaging 38(6):1175–1188. https://doi.org/10.1007/s00259-011-1811-3

Kenny RW, Ackery DM, Fleming JS, Goddard BA, Grant RW (1975) Deconvolution analysis of the scintillation camera renogram. Br J Radiol 48(570):481–486. https://doi.org/10.1259/0007-1285-48-570-481

Khalighi MM, Deller TW, Fan AP, Gulaka PK, Shen B, Singh P et al (2018) Image-derived input function estimation on a TOF-enabled PET/MR for cerebral blood flow mapping. J Cereb Blood Flow Metab 38(1):126–135. https://doi.org/10.1177/0271678x17691784

Rebelos E, Mari A, Oikonen V, Iida H, Nuutila P, Ferrannini E (2023) Evaluation of renal glucose uptake with [18F]FDG-PET: methodological advancements and metabolic outcomes. Metabolism 141:155382. https://doi.org/10.1016/j.metabol.2022.155382

Richardson WH (1972) Bayesian-based iterative method of image restoration. J Opt Soc Am 62(1):55. https://doi.org/10.1364/josa.62.000055

Werner RA, Chen X, Lapa C, Koshino K, Rowe SP, Pomper MG et al (2019) The next era of renal radionuclide imaging: novel PET radiotracers. Eur J Nucl Med Mol Imaging 46(9):1773–1786

Werner RA, Ordonez AA, Sanchez-Bautista J, Marcus C, Lapa C, Rowe SP, Pomper MG, Leal JP, Lodge MA, Javadi MS, Jain SK, Higuchi T (2019) Novel functional renal PET imaging with 18F-FDS in human subjects. Clin Nucl Med 44(5):410–411. https://doi.org/10.1097/rlu.0000000000002494

Publisher's Note